Rare Metal Materials and Engineering
Volume 52, Issue 11, November 2023
Available online at www.rmme.ac.cn

Science Press

Cite this article as: Zhang Yuhan, Jin Na, Liu Ying. Doping Effects of Mo_2CoB_2 Ternary Transition Metal Boride: a First-Principles Study[J]. Rare Metal Materials and Engineering, 2023, 52(11): 3748-3756. DOI: 10.12442/j.issn.1002-185X.20230245.

ARTICLE

Doping Effects of Mo_2CoB_2 Ternary Transition Metal Boride: a First-Principles Study

Zhang Yuhan, Jin Na, Liu Ying

Center for Rare Earth & Vanadium & Titanium Materials, College of Materials Science and Engineering, Sichuan University, Chengdu 610065, China

Abstract: The first-principles calculation was used to investigate the influence of doping fourth-period transition metal elements on the structural, mechanical, and thermal properties of Mo_2CoB_2. Through the calculation of cohesive energy and formation enthalpy as well as the calculation comparison between the obtained results and Born-Huang criterion, all doped compounds are thermodynamically and mechanically stable. Point defect theory was employed to determine the occupation sites and occupation preference of doped elements in the Mo_2CoB_2 crystal cell. Results show that Sc and Ti exhibit strong preference for Mo sites, and V has a weak preference for Mo sites. Additionally, Cr, Mn, Fe, Cu, and Zn have a weak preference for Co sites, and Ni has a strong preference for Co sites. Debye temperatures were obtained by the contrast calculation. The results reveal that except $Mo_7TiCo_4B_8$, $Mo_7VCo_4B_8$, and $Mo_7CrCo_4B_8$, the doped models all have lower Debye temperatures than the undoped model, suggesting that except Ti, V, and Cr elements, the addition of transition metal elements of large quantity into the Mo_2CoB_2 hard phase should be avoided. Furthermore, except that of the Cr-doped model, the hardness of the doped models is lower than that of the undoped model, and the models with doped elements at preferential sites normally exhibit higher hardness than those at non-preferred sites do. This research provides theoretical basis for the development of Mo_2CoB_2-Co cermet with improved properties.

Key words: cermet; first-principles; mechanical properties; Mo_2CoB_2-Co

Cermet is a non-homogeneous composite material composed of metal or alloy with various ceramic phases[1–2], which not only has excellent metal properties, such as ductility and plasticity, but also presents good ceramic properties, such as high strength, great hardness, high wear resistance, and fine temperature resistance[3–4]. The cermet applications in tool materials and structural materials become more and more important, promoting the industrial development and improving the productivity.

WC-Co is one of the commonly used cermets due to its high hardness, toughness, and corrosion resistance[5], and it has been widely used as tool material, such as milling cutter, boring tool, turning tool, planer, and drill, to cut non-ferrous metals, cast iron, plastics, synthetic fibers, graphite, glass, stone, stainless steel, and high manganese steel. However, the raw material tungsten is a global strategic non-renewable resource[6], and the fracture toughness of WC-Co is relatively low, resulting in the difficulty of W resource access and the easy occurrence of crack initiation under complex stress conditions[7]. Therefore, tungsten-free cermet materials with high hardness and high toughness are urgently required.

Three generations of tungsten-free cermet materials have been developed[8]. The first-generation cermet is produced from Ni-doped TiC. The second-generation tungsten-free cermet is prepared by adding Mo element into the Ni-doped TiC phase, which improves the wettability and toughness. The third-generation tungsten-free cermet is prepared by adding nitrides into the hard phase to form a composite phase. The binder phase performance is enhanced by adding Co and other elements. Although the Ti(C, N) -based cermet exhibits good high-temperature hardness and excellent wear resistance, its lower toughness restricts the further application. Therefore, the tungsten-free cermet materials with excellent properties should be further developed.

Received date: April 24, 2023
Foundation item: National Natural Science Foundation of China (U21A2053)
Corresponding author: Jin Na, Ph. D., Associate Professor, Center for Rare Earth & Vanadium & Titanium Materials, College of Materials Science and Engineering, Sichuan University, Chengdu 610065, P. R. China, E-mail: jinna319@scu.edu.cn

Currently, the ternary transition metal boride with excellent abrasion resistance, good corrosion resistance, and relatively good mechanical properties at high temperatures attracts much attention in the research of tungsten-free cermet[9], which mainly involves the Mo_2FeB_2-Fe, Mo_2NiB_2-Ni, and WCoB-Co[10]. Among them, the ternary boride Mo_2FeB_2-Fe[11] has high wear resistance, Mo_2NiB_2-Ni[12] has remarkable corrosion resistance, and WCoB-Co[13] has exceedingly high-temperature resistance. In addition to these ternary borides, Mo_2CoB_2-Co is also worthy of attention: it is tungsten-free and its binder phase Co has higher corrosion resistance than Fe and Ni do. Although the ternary borides show great performance in various applications, the brittleness is still a problem[14]. Therefore, the method of doping alloying elements is proposed to improve the cermet microstructure and to enhance the mechanical properties. Mo_2CoB_2-Co cermet is mainly composed of the hard phase Mo_2CoB_2 which directly affects the wear resistance and thermal properties of cermet. Therefore, the effects of transition metal elements doping on the mechanical and thermal properties of Mo_2CoB_2 hard phase should be thoroughly investigated.

The first-principles calculations have been widely employed to study the mechanical and thermal properties of materials. Zhang et al[15] used the first-principles method to investigate the elastic properties, thermodynamic properties, and electronic structure of AgAuPd medium entropy alloy under different pressures, providing theoretical basis for the experiments. Lin[16] and Wang[17] et al used the first-principles study to analyze the effects of Cr, Ni, and Mn elements on the crystal structure and mechanical properties of Mo_2FeB_2. It is found that Cr, Ni, and Mn tend to occupy the Fe sites in Mo_2FeB_2. Cr can significantly increase the shear modulus, Young's modulus, and Vickers hardness of Mo_2FeB_2, whereas Ni reduces the values of the abovementioned properties. However, Ni can improve the ductility of Mo_2FeB_2. Zhang et al[18–20] used the first-principles calculations to study the effects of doped Cr, Mn, V, and other transition metal elements on the crystal structure, mechanical properties, and electronic structure of WCoB. It is demonstrated that Cr, Mn, and V can reduce the shear modulus and bulk modulus of WCoB to a certain extent.

Therefore, in this research, the first-principles calculation was used to calculate the cohesive energy and enthalpy of Mo_2CoB_2 supercells doped with the fourth-period transition metal elements. The atomic sites of various doping elements in the Mo_2CoB_2 supercells were analyzed, and the effects of the doping elements on crystal structure, mechanical properties, and thermal properties of Mo_2CoB_2 were investigated.

1 First-Principles Calculation

Before constructing the transition metal element-doped Mo_2CoB_2 model, two issues should be considered: the doping concentration and doping site. Through the comprehensive consideration, a supercell model (20 atoms) of 1×2×1 of Mo_2CoB_2 crystal was selected in this research. Besides, the doped models were constructed with the transition metal (Sc, Ti, V, Cr, Mn, Fe, Ni, Cu, Zn) atoms occupying both Mo and Co sites, and the specific doping sites need to be determined based on the results of first-principles calculations. The schematic diagrams of doped models are shown in Fig.1a–1b, and the doped atoms occupying the Mo and Co sites are represented by $X_{Mo\text{-}site}$ and $X_{Co\text{-}site}$, respectively. In addition, the anti-site models with a single Mo atom occupying Co site and a single Co atom occupying the Mo site were constructed, as well as vacancy models with vacancies at the Mo and Co sites, as shown in Fig.1c–1f.

All first-principles calculations were conducted based on the density functional theory[21–22] with the Vienna Ab Initio Simulation Package[23–24]. The interactions between the atomic core and the valence electron were described by the Projector Augmented Wave potentials[25–26]. The exchange and correlation functions were evaluated through the Perdew-Burke-Ernzerh function with generalized gradient approximation[27]. The cut-off energy of the plane wave was 500 eV. Monkhorst-Pack type k-points grid was used and the number of k-points was 6×6×6. The self-consistent field converged below 1×10^{-5} eV/atom. The maximum force tolerance was below 1×10^{-1} eV/nm.

2 Results and Discussion

2.1 Structural stability

In order to investigate the positions of doped elements, several criteria methods based on atomic radius[18], enthalpy of formation, and cohesive energy[28] are proposed.

Table 1 presents the atomic radii of Mo and the fourth-period elements. According to the atomic radius-based occupancy criterion, the closer the distance between the transition metal element and Mo (or Co) element, the higher the occupancy probability of the Mo (or Co) site by the transition metal element[18]. The eigenvalue $R_X - 1/2(R_{Mo}+R_{Co})$ is introduced to determine the critical distance between the transition metal element X and Mo/Co, where R_X is the atomic radius of the transition metal element X, R_{Mo} is the atomic radius of the Mo element, and R_{Co} is the atomic radius of Co element. If $R_X - 1/2(R_{Mo}+R_{Co})>0$, the atomic radius of X element is closer to Mo; otherwise, the atomic radius of X element is closer to that of Co. As shown in Table 1, Sc, Ti, V, and Zn elements tend to occupy the Mo sites, whereas Cr, Mn, Fe, Ni, and Cu elements tend to occupy the Co sites.

The cohesive energy can also be used to determine the positions of doped elements. Lin et al[16] studied the doping positions of Cr, Ni, and Mn elements in Mo_2FeB_2 by cohesive energy. It is found that the cohesive energy of Cr, Ni, and Mn elements occupying the Fe sites is lower than that occupying the Mo sites, indicating that Cr, Ni, and Mn elements tend to occupy the Fe sites. Keränen et al[29] proved that the Cr element does not only occupy the Fe sites in Mo_2FeB_2. Some Cr atoms also occupy the Mo sites. It is clear that the cohesive energy-based method is not accurate. Compared to the cohesive energy, the enthalpy of formation as the

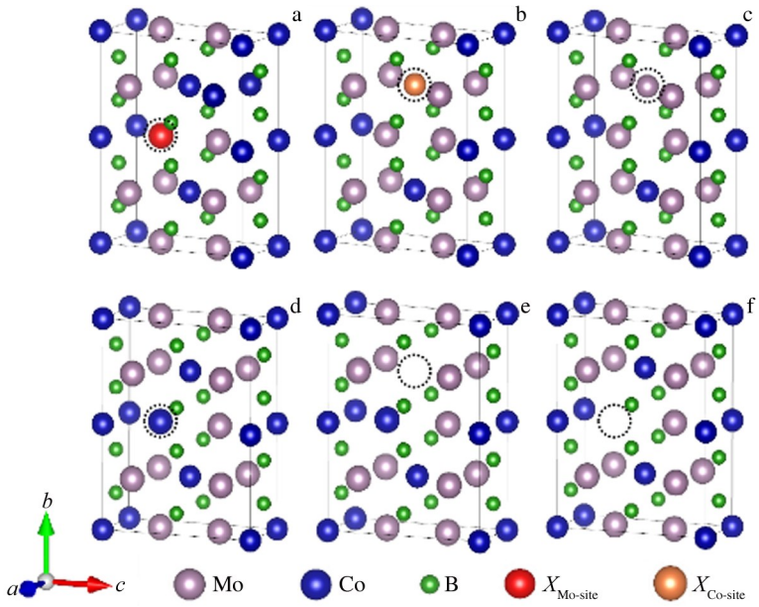

Fig.1 Schematic diagrams of point defect models of Mo_2CoB_2 supercell: (a) $Mo_7XCo_4B_8$ with transition metal element *X* occupying Mo site; (b) $Mo_8Co_3XB_8$ with transition metal element *X* occupying Co site; (c) $Mo_9Co_3B_8$ with Mo element occupying Co site; (d) $Mo_7Co_5B_8$ with Co element occupying Mo site; (e) $Mo_7Co_4B_8$ with vacancy occupying Mo site; (f) $Mo_8Co_3B_8$ with vacancy occupying Co site (dashed circle indicates the site changes)

determination criterion of dopant elements is more reliable. Table 2 shows the lattice parameters, cohesive energies, and enthalpies of formation of undoped and doped transition metal models. In this research, the cohesive energy and formation enthalpy can be calculated by Eq. (1) and Eq. (2) [30], respectively:

$$E_{coh}(Mo_aCo_bX_cB_d)=\frac{E_{tot}(Mo_aCo_bX_cB_d)-aE(Mo)-bE(Co)-cE(X)-dE(B)}{a+b+c+d} \quad (1)$$

$$\Delta H_r(Mo_aCo_bX_cB_d)=E_{coh}(Mo_aCo_bX_cB_d)-aE_{coh}(Mo)-bE_{coh}(Co)-cE_{coh}(X)-dE_{coh}(B) \quad (2)$$

where $E_{coh}(Mo_aCo_bX_cB_d)$ and $\Delta H_r(Mo_aCo_bX_cB_d)$ are the cohesive energy and enthalpy of formation of $Mo_aCo_bX_cB_d$ compounds (*X* indicates the doped transition metal element); $E_{tot}(Mo_aCo_bX_cB_d)$ is the total energy of $Mo_aCo_bX_cB_d$ molecule; *E*(Mo), *E*(Co), *E*(*X*), and *E*(*B*) are the energies of free Mo, Co, *X*, and B atoms, respectively; E_{coh}(Mo), E_{coh}(Co), E_{coh}(*X*), and E_{coh}(B) are the cohesive energies of Mo, Co, *X*, and B per atom, respectively. According to Table 2, all cohesive energy and enthalpy of formation are negative, indicating that all the compounds are thermodynamically stable. It can be seen that when Sc, Ti, V, and Cr elements occupy the Mo sites, their enthalpies of formation are smaller than those when they occupy the Co sites. When Mn, Fe, Ni, Cu, and Zn elements occupy the Co sites, their enthalpies of formation are smaller than those when they occupy the Mo sites. Hence, Sc, Ti, V, and Cr elements tend to occupy the Mo sites, whereas the Mn, Fe, Ni, Cu, and Zn elements tend to occupy the Co sites.

Table 1 Atomic radii, calculated eigenvalue, and preferential sites of the fourth-period elements and Mo element

Element	Atomic radius/nm	$R_x-1/2(R_{Mo}+R_{Co})$	Preferential site
Mo	0.139	7	Mo
Sc	0.162	30	Mo
Ti	0.147	15	Mo
V	0.134	2	Mo
Cr	0.128	−4	Co
Mn	0.127	−5	Co
Fe	0.126	−6	Co
Co	0.125	−7	Co
Ni	0.124	−8	Co
Cu	0.128	−4	Co
Zn	0.134	2	Mo

The abovementioned criteria only consider the single factor and do not take into account the vacancy movement and atomic migration in the material. Currently, the widely accepted theory is the point defect theory[31–32], whose predictions show good consistency with the experiments[33–35]. Therefore, the site occupancy by transition metal atoms in Mo_2CoB_2 crystal is further discussed based on this theory.

In this research, the point defects in Mo_2CoB_2 crystal can be divided into six types: (1) the transition metal atom *X* occupying the Mo site, as denoted by X_{Mo}; (2) the transition metal atom *X* occupying the Co site, as denoted by X_{Co}; (3) Mo atom enrichment in Mo_2CoB_2 crystal with Mo atom occupying the Co site, as denoted by Mo_{Co}; (4) Co atom enrichment in Mo_2CoB_2 crystal with Co atom occupying the Mo site, as denoted by Co_{Mo}; (5) a vacancy occupying the Mo site, as

Table 2 Lattice parameters, cohesive energies, and enthalpies of formation of $Mo_aCo_bX_cB_d$ compounds with undoped, doped, and vacancy models

Compound	Lattice parameter/nm			Cell volume/$\times10^{-3}$ nm^{-3}	Cohesive energy, E_{coh}/eV·atom^{-1}	Enthalpy of formation, ΔH_r/eV·molecule^{-1}
	a	*b*	*c*			
$Mo_8Co_4B_8$	0.7113	0.9117	0.3163	205.12	−7.123	−9.137
$Mo_7Co_4B_8$	0.7073	0.9030	0.3141	200.63	−6.944	−6.190
$Mo_8Co_3B_8$	0.7043	0.9067	0.3146	200.90	−7.133	−7.536
$Mo_7Co_5B_8$	0.7064	0.9052	0.3150	201.43	−6.991	−8.758
$Mo_9Co_3B_8$	0.7214	0.9315	0.3156	212.11	−7.210	−8.624
$Mo_7ScCo_4B_8$	0.7161	0.9157	0.3178	208.40	−6.987	−9.865
$Mo_8Co_3ScB_8$	0.7136	0.9381	0.3210	214.88	−7.000	−7.867
$Mo_7TiCo_4B_8$	0.7110	0.9112	0.3165	205.06	−7.088	−10.724
$Mo_8Co_3TiB_8$	0.7119	0.9308	0.3186	211.15	−7.134	−9.397
$Mo_7VCo_4B_8$	0.7079	0.9084	0.3155	202.92	−7.067	−10.194
$Mo_8Co_3VB_8$	0.7133	0.9252	0.3161	208.59	−7.148	−9.570
$Mo_7CrCo_4B_8$	0.7067	0.9066	0.3149	201.75	−7.035	−9.398
$Mo_8Co_3CrB_8$	0.7146	0.9217	0.3142	206.92	−7.146	−9.371
$Mo_7MnCo_4B_8$	0.7064	0.9053	0.3147	201.27	−6.934	−9.098
$Mo_8Co_3MnB_8$	0.7128	0.9170	0.3154	206.17	−7.072	−9.611
$Mo_7FeCo_4B_8$	0.7056	0.9045	0.3153	201.22	−6.974	−8.792
$Mo_8Co_3FeB_8$	0.7116	0.9125	0.3162	205.33	−7.130	−9.654
$Mo_7NiCo_4B_8$	0.7075	0.9053	0.3150	201.77	−6.965	−8.011
$Mo_8Co_3NiB_8$	0.7112	0.9120	0.3170	205.59	−7.131	−9.762
$Mo_7CuCo_4B_8$	0.7093	0.9059	0.3161	203.10	−6.858	−7.928
$Mo_8Co_3CuB_8$	0.7116	0.9148	0.3177	206.81	−7.014	−8.795
$Mo_7ZnCo_4B_8$	0.7115	0.9063	0.3178	204.89	−6.732	−7.811
$Mo_8Co_3ZnB_8$	0.7109	0.9184	0.3195	208.58	−6.872	−8.353

denoted by Va_{Mo}; (6) a vacancy occupying the Co site, as denoted by Va_{Co}. Thus, the enthalpy of formation of $Mo_8Co_3XB_8$ and $Mo_7XCo_4B_8$ compounds containing point defects can be represented as a linear function of defect atom concentrations, as follows:

$$\Delta H = \Delta H(Mo_8Co_4B_8) + \sum_d H_d X_d \quad (3)$$

where X_d is the defect concentration of type d={X_{Mo}, X_{Co}, Mo_{Co}, Co_{Mo}, Va_{Mo}, Va_{Co}}, $\Delta H(Mo_8Co_4B_8)$ is the enthalpy of formation for $Mo_8Co_4B_8$ compound, and H_d is the enthalpy of formation for d type defect. Therefore, the enthalpy of formation for the $Mo_{8-x}Co_{4-y}BX_{x+y}$ (x and y represent the numbers of missing Mo and Co atoms relative to the defect-free Mo_2CoB_2 crystal, respectively, and $x+y$ is the total number of defect atoms) compound containing point defects can be calculated by Eq.(4), as follows:

$$\Delta H(Mo_{8-x}Co_{4-y}B_8X_{x+y}) = E(Mo_{8-x}Co_{4-y}B_8X_{x+y}) - (8-x)E(Mo) - (4-y)E(Co) - 8E(B) - (x+y)E(X) \quad (4)$$

where $E(Mo_{8-x}Co_{4-y}B_8X_{x+y})$ is the total energy of $Mo_{8-x}Co_{4-y}B_8X_{x+y}$; E(Mo), E(Co), E(X), and E(B) are the ground state energies of the pure Mo, Co, X, and B elements, respectively.

Based on Eq.(3−4), the enthalpy of formation for models with point defects can be described:

$$H_d = \frac{\Delta H(Mo_{8-x}Co_{4-y}B_8X_{x+y}) - \Delta H(Mo_8Co_4B_8)}{X_d} \quad (5)$$

The 1×2×1 Mo_2CoB_2 supercell was used. When the defect types are doping defects and anti-site defects, the X_d value is 20; when the vacancy defects occur, the X_d value is 19. The energy required to move the transition metal atom X from the Mo site to the Co site in the Mo_2CoB_2 supercell is denoted as $E_X^{Mo\rightarrow Co}$, and its expression is as follows:

$$E_X^{Mo\rightarrow Co} = E(Mo_8Co_3XB_8) - E(Mo_7XCo_4B_8) + E(Mo_7Co_5B_8) - E(Mo_8Co_4B_8) \quad (6)$$

If $E_X^{Mo\rightarrow Co} < 0$, $E(Mo_7XCo_4B_8)+E(Mo_8Co_4B_8) > E(Mo_8Co_3XB_8)+E(Mo_7Co_5B_8)$. Thus, the energy of $E(X_{Co})+E(Co_{Mo})$ is less than the energy of $E(X_{Mo})+E(Co_{Co})$. This result indicates that when X moves from the Mo site to the Co site, the total energy of the system is reduced, and therefore the transition metal atom X prefers to occupy the Co site. If $E_X^{Mo\rightarrow Co} < E(Va_{Mo}) + E(Va_{Co})$, the transition metal atom X prefers to occupy the Mo site, because the energy required for the X atom movement from Mo site to Co site is less than the anti-site exchange formation energy E^{ant}, where $E^{ant}=E(Va_{Mo})+E(Va_{Co})$. In both cases, the atom shows a strong site preference. However, between 0 and E^{ant}, the weak site preference region also exists. Therefore, $E_X^{Mo\rightarrow Co}$ can be normalized by E^{ant}, as follows:

$$\tilde{E}_X^{\mathrm{Mo}\rightarrow\mathrm{Co}} = \frac{E_X^{\mathrm{Mo}\rightarrow\mathrm{Co}}}{E^{\mathrm{ant}}} \quad (7)$$

Finally, the occupancy of transition metal atoms can be divided into four situations: (1) $\tilde{E}_X^{\mathrm{Mo}\rightarrow\mathrm{Co}} < 0$, strong Co site preference; (2) $\tilde{E}_X^{\mathrm{Mo}\rightarrow\mathrm{Co}} > 1$, strong Mo site preference; (3) $0 < \tilde{E}_X^{\mathrm{Mo}\rightarrow\mathrm{Co}} < 0.5$, weak Co site preference; (4) $0.5 < \tilde{E}_X^{\mathrm{Mo}\rightarrow\mathrm{Co}} < 1$, weak Mo site preference.

Taking the data in Table 2 into the abovementioned formulas, $\tilde{E}_X^{\mathrm{Mo}\rightarrow\mathrm{Co}}$ values can be calculated, and the results are shown in Fig.2. It can be seen that Sc and Ti exhibit a strong Mo site preference, whereas V exhibits a weak Mo site preference. Cr, Mn, Fe, Cu, and Zn show weak Co site preference, and Ni shows a strong Co site preference. The larger the $\tilde{E}_X^{\mathrm{Mo}\rightarrow\mathrm{Co}}$ value, the stronger the preference of transition metal element occupying the Mo site. The smaller the $\tilde{E}_X^{\mathrm{Mo}\rightarrow\mathrm{Co}}$ value, the stronger the preference of transition metal element occupying the Co sit. Additionally, with increasing the atomic number, the $\tilde{E}_X^{\mathrm{Mo}\rightarrow\mathrm{Co}}$ value of the fourth-period transition metal element X is decreased firstly and then increased. The lowest $\tilde{E}_X^{\mathrm{Mo}\rightarrow\mathrm{Co}}$ value appears when X is Ni element. Therefore, the Ni element has the strongest preference to occupy the Co site, and the Sc element has the strongest preference to occupy the Mo site.

It can be seen that the atomic radius-based criterion cannot quantitatively present the strength of atomic site preference and cannot comprehensively consider the influencing factors, such as doping element concentration and temperature. It can only roughly predict the specific atomic site preference. In most cases, the results obtained by the atomic radius-based criterion are consistent with the predictions obtained by point defect theory, except for the site preference of Zn element. The cohesive energy-based criterion is theoretically inconsistent with experiment conditions, so it cannot be used as the criterion. Moreover, the enthalpy of formation criterion also predicts different results for Cr element.

2.2 Mechanical properties

Before the mechanical property analysis, the traditional mechanical stability conditions should be considered. The elastic constants C_{ij} of $Mo_aCo_bX_cB_d$ compounds with undoped, doped, and vacancy models are shown in Table 3. For

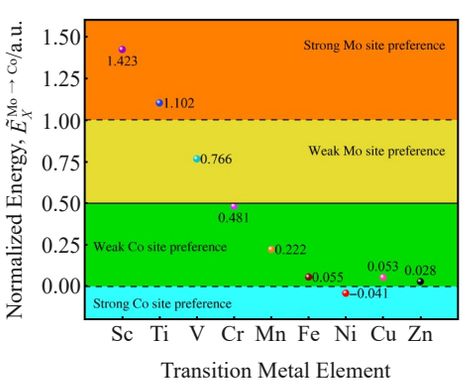

Fig.2 Site preference distributions of doped transition element X of the fourth-period in Mo_2CoB_2 supercells

Table 3 Elastic constants C_{ij} of $Mo_aCo_bX_cB_d$ compounds with undoped, doped, and vacancy models

Compound	C_{11}	C_{22}	C_{33}	C_{44}	C_{55}	C_{66}	C_{12}	C_{13}	C_{23}
$Mo_8Co_4B_8$	551	560	532	226	226	205	155	226	214
$Mo_7ScCo_4B_8$	507	485	526	212	186	206	205	150	197
$Mo_8Co_3ScB_8$	476	498	480	209	199	26	130	200	196
$Mo_7TiCo_4B_8$	542	505	545	221	198	214	217	151	207
$Mo_8Co_3TiB_8$	498	515	521	86	218	207	220	205	154
$Mo_7VCo_4B_8$	542	552	512	227	218	200	149	220	216
$Mo_8Co_3VB_8$	530	549	500	227	208	137	158	229	218
$Mo_7CrCo_4B_8$	545	521	552	226	191	219	229	152	211
$Mo_8Co_3CrB_8$	542	561	522	232	215	178	160	230	222
$Mo_7MnCo_4B_8$	528	537	499	223	216	185	151	226	209
$Mo_8Co_3MnB_8$	553	545	485	231	218	192	152	223	207
$Mo_7FeCo_4B_8$	530	535	523	214	210	172	152	240	215
$Mo_8Co_3FeB_8$	557	527	556	233	201	219	228	156	220
$Mo_7NiCo_4B_8$	504	513	497	211	201	168	156	224	208
$Mo_8Co_3NiB_8$	539	551	528	216	227	194	156	230	206
$Mo_7CuCo_4B_8$	505	503	492	209	193	161	157	217	202
$Mo_8Co_3CuB_8$	523	538	516	208	227	181	151	230	205
$Mo_7ZnCo_4B_8$	486	506	494	205	197	153	161	212	207
$Mo_8Co_3ZnB_8$	512	523	509	204	223	167	151	225	195

orthorhombic crystals with nine independent elastic stiffness constants, according to Born-Huang's theory[36], the criterion can be expressed as follows:

$$\begin{cases} C_{11} > 0, C_{44} > 0, C_{55} > 0, C_{66} > 0, C_{11}C_{22} > C_{12}^2 \\ C_{11}C_{22}C_{33} + 2C_{12}C_{13}C_{23} - C_{11}C_{23}^2 - C_{22}C_{13}^2 - C_{33}C_{12}^2 \end{cases} \quad (8)$$

By substituting the elastic constants C_{ij} in Table 3 into Eq. (8), it can be seen that all the compounds satisfy the criterion, indicating that these crystals are all mechanically stable. For orthorhombic crystals, the related parameters can be calculated by Eq.(9–12)[37–39], as follows:

$$B_{\mathrm{V}} = \frac{1}{9}(C_{11} + C_{22} + C_{33}) + \frac{2}{9}(C_{12} + C_{23} + C_{13}) \quad (9)$$

$$\frac{1}{B_{\mathrm{R}}} = (S_{11} + S_{22} + S_{33}) + 2(S_{12} + S_{23} + S_{13}) \quad (10)$$

$$G_{\mathrm{V}} = \frac{1}{15}(C_{11} + C_{22} + C_{33}) - \frac{1}{15}(C_{12} + C_{23} + C_{13}) + \frac{1}{5}(C_{44} + C_{55} + C_{66}) \quad (11)$$

$$\frac{1}{G_{\mathrm{R}}} = \frac{4}{15}(S_{11} + S_{22} + S_{33}) - \frac{4}{15}(S_{12} + S_{23} + S_{13}) + \frac{1}{5}(S_{44} + S_{55} + S_{66}) \quad (12)$$

where S_{ij} is the elastic compliant coefficient which can be converted from the corresponding C_{ij} matrix; B is bulk modulus; G is shear modulus; the subscripts V and R indicate the Voigt constraint and Reuss constraint, respectively. The bulk modulus B and shear modulus G can be calculated by Voigt-Reuss-Hill approximations[40], namely B_{VRH} and G_{VRH}, respectively:

$$B_{VRH} = \frac{1}{2}(B_V + B_R) \quad (13)$$

$$G_{VRH} = \frac{1}{2}(G_V + G_R) \quad (14)$$

According to the calculated elastic modulus, Young's modulus E and Poisson's ratio υ can be calculated from the bulk modulus and shear modulus[41]. Moreover, the Vickers hardness H_V can be deduced by the empirical formula[42], as follows:

$$E = \frac{9B_{VRH}G_{VRH}}{3B_{VRH} + G_{VRH}} \quad (15)$$

$$\upsilon = \frac{3B_{VRH} - 2G_{VRH}}{2(3B_{VRH} + G_{VRH})} \quad (16)$$

$$H_V = 2(K^2G_{VRH})^{0.585} - 3 \quad (17)$$

$$K = \frac{G_{VRH}}{B_{VRH}} \quad (18)$$

where K is the Pugh's modulus ratio. Table 4 shows the results of bulk modulus B, shear modulus G, Young's modulus E, Poisson's ratio υ, B/G value, and hardness H_V of $Mo_aCo_bX_cB_d$ compounds with undoped, doped, and vacancy models. The B/G value is commonly used as a criterion to evaluate the brittleness and ductility of material: the larger the B/G value, the better the material ductility[43]. Usually, the materials with the B/G value greater than 1.75 are considered as ductile materials.

Fig.3 shows B/G values of doped transition metal element X at different sites in the Mo_2CoB_2 supercell. It can be seen that when the transition metal elements occupy the Mo site, the B/G value of the crystal is generally increased with increasing the atomic number, indicating the increasing ductility. When the transition metal elements occupy the Co site, the B/G value of the crystal is decreased with the increasing the atomic number, presenting the decline in ductility. Moreover, the B/G values of all doped models are higher than those of the undoped model, suggesting that doping transition metal elements can improve the ductility of Mo_2CoB_2. It is worth noting that when the Sc, Ti, and V elements occupy the Co site, their B/G values are greater than 1.75. However, it is already found that Sc, Ti, and V tend to occupy the Mo site. Therefore, these three models cannot be used as reference.

2.3 Debye temperature

Debye temperature Θ_D is related to many physical properties of crystal, such as lattice vibration, thermal conductivity, thermal expansion coefficient, and heat capacity. With previously calculated bulk modulus B and shear modulus G, the longitudinal sound velocity v_l, the transverse sound velocity v_t, the average sound velocity v_m, and Debye temperature Θ_D of the doped models can be calculated by Eq.(19–22)[44–45], as follows:

$$v_l = \sqrt{(B_{VRH} + \frac{4}{3}G_{VRH})\frac{1}{\rho}} \quad (19)$$

$$v_t = \sqrt{(G_{VRH})\frac{1}{\rho}} \quad (20)$$

$$v_m = \left[\frac{1}{3}\left(\frac{1}{v_l^3} + \frac{1}{v_t^3}\right)\right]^{-\frac{1}{3}} \quad (21)$$

$$\Theta_D = \frac{h}{k_B}\left[\frac{3n}{4\pi}\left(\frac{n_A\rho}{M}\right)\right]^{\frac{1}{3}} v_m \quad (22)$$

Table 4 Bulk modulus B, shear modulus G, Young's modulus E, Poisson's ratio υ, B/G value, and Vickers hardness H_V of $Mo_aCo_bX_cB_d$ compounds with undoped, doped, and vacancy models

Compound	B_V	B_R	B_{VRH}	G_V	G_R	G_{VRH}	E/GPa	υ	B/G	H_V/GPa
$Mo_8Co_4B_8$	314.8	314.3	314.6	201.2	196.5	198.9	492.7	0.239	1.58	22.9
$Mo_7ScCo_4B_8$	291.3	291.2	291.2	185.4	181.2	183.3	454.6	0.240	1.59	21.5
$Mo_8Co_3ScB_8$	278.4	277.3	277.8	148.8	81.4	115.1	303.4	0.318	2.41	9.1
$Mo_7TiCo_4B_8$	304.8	304.6	304.7	194.6	189.9	192.3	476.5	0.239	1.59	22.3
$Mo_8Co_3TiB_8$	299.0	298.5	298.7	166.1	147.6	156.8	400.4	0.277	1.91	15.4
$Mo_7VCo_4B_8$	308.1	307.8	308.0	197.1	191.6	194.3	481.7	0.239	1.59	22.5
$Mo_8Co_3VB_8$	309.9	309.7	309.8	179.3	171.0	175.2	442.1	0.262	1.77	18.3
$Mo_7CrCo_4B_8$	311.5	311.0	311.2	195.5	190.3	192.9	479.6	0.243	1.61	21.9
$Mo_8Co_3CrB_8$	316.6	316.3	316.5	192.4	186.8	189.6	474.1	0.25	1.67	20.7
$Mo_7MnCo_4B_8$	303.8	303.4	303.6	190.0	184.0	187.0	465.4	0.245	1.62	21.3
$Mo_8Co_3MnB_8$	305.2	305.2	305.2	194.9	188.1	191.5	475.1	0.241	1.59	22.1
$Mo_7FeCo_4B_8$	311.3	310.1	310.7	184.5	179.3	181.9	456.6	0.255	1.71	19.6
$Mo_8Co_3FeB_8$	316.3	315.9	316.1	199.6	194.3	197.0	489.3	0.242	1.61	22.3
$Mo_7NiCo_4B_8$	298.9	298.3	298.6	177.8	172.9	175.4	440.0	0.254	1.70	19.2
$Mo_8Co_3NiB_8$	311.5	311.0	311.2	195.8	191.2	193.5	480.8	0.243	1.61	22.0
$Mo_7CuCo_4B_8$	294.5	294.0	294.3	174.5	170.4	172.5	432.9	0.255	1.71	18.9
$Mo_8Co_3CuB_8$	305.4	304.7	305.1	189.4	184.2	186.8	465.4	0.246	1.63	21.1
$Mo_7ZnCo_4B_8$	293.9	293.2	293.6	169.5	165.8	167.6	422.5	0.26	1.75	17.9
$Mo_8Co_3ZnB_8$	298.5	297.8	298.1	183.5	178.5	181.0	451.7	0.248	1.65	20.4

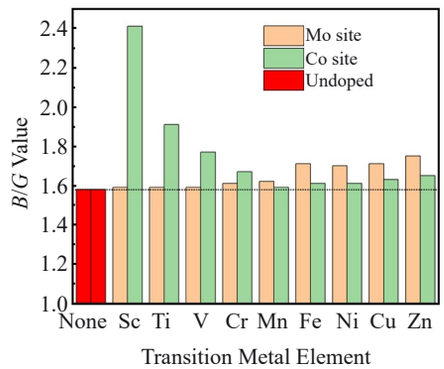

Fig.3 *B*/*G* values of doped transition metal element *X* at different sites in Mo_2CoB_2 supercell (dashed line represents the *B*/*G* value of undoped model)

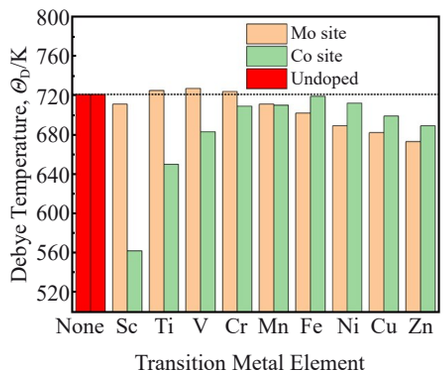

Fig.4 Debye temperatures of doped transition metal element *X* at different sites in Mo_2CoB_2 supercell (dashed line represents Debye temperature value of undoped model)

where *h* is Planck's constant, k_B is Boltzmann's constant, *n* is the number of atoms per formula unit, n_A is Avogadro's number, ρ is the density, and *M* is the molecular weight. The calculated results of these parameters are shown in Table 5, and the Debye temperatures of doped transition metal element *X* at different sites in the Mo_2CoB_2 supercell are shown in Fig.4.

According to Fig. 4, the Debye temperature of each doped model is firstly increased and then decreased with increasing the atomic number. When the transition metal element occupies the Mo site, the maximum Debye temperature is obtained for the V element; when the transition metal element occupies the Co site, the maximum Debye temperature is obtained for the Fe element. It can be seen that all transition metal elements tend to have a higher Debye temperature when they occupy their preferred sites. For example, the Debye temperatures of Sc (strong), Ti (strong), and V (weak) elements occupying the Mo sites are much higher than those occupying the Co sites. In contrast, the Debye temperatures of Fe (weak), Ni (strong), Cu (weak), and Zn (weak) elements occupying the Co sites are much higher than those occupying the Mo sites. Moreover, the Debye temperatures of $Mo_7TiCo_4B_8$, $Mo_7VCo_4B_8$, and $Mo_7CrCo_4B_8$ are higher than those of the undoped model, and the Debye temperatures of other doped models show lower Debye temperatures.

Table 5 Longitudinal phonon velocity v_l, transverse phonon velocity v_t, average phonon velocity v_m, and Debye temperature Θ_D of $Mo_aCo_bX_cB_d$ compounds with undoped, doped, and vacancy models

Compound	v_l/m·s^{-1}	v_t/m·s^{-1}	v_m/m·s^{-1}	Θ_D/K
$Mo_8Co_4B_8$	8106	4748	5264	721
$Mo_7ScCo_4B_8$	8045	4706	5219	711
$Mo_8Co_3ScB_8$	7203	3721	4166	562
$Mo_7TiCo_4B_8$	8155	4774	5293	725
$Mo_8Co_3TiB_8$	7737	4300	4789	650
$Mo_7VCo_4B_8$	8144	4767	5286	727
$Mo_8Co_3VB_8$	7943	4510	5014	683
$Mo_7CrCo_4B_8$	8126	4734	5251	724
$Mo_8Co_3CrB_8$	8093	4671	5186	709
$Mo_7MnCo_4B_8$	7994	4649	5158	711
$Mo_8Co_3MnB_8$	8006	4679	5189	710
$Mo_7FeCo_4B_8$	7992	4582	5090	702
$Mo_8Co_3FeB_8$	8115	4734	5251	719
$Mo_7NiCo_4B_8$	7840	4500	4998	689
$Mo_8Co_3NiB_8$	8042	4689	5201	712
$Mo_7CuCo_4B_8$	7787	4467	4962	682
$Mo_8Co_3CuB_8$	7941	4611	5116	699
$Mo_7ZnCo_4B_8$	7761	4419	4912	673
$Mo_8Co_3ZnB_8$	7863	4554	5055	689

2.4 Hardness

Hardness is a key factor influencing the wear resistance of cermet materials. The hardness of doped Mo_2CoB_2 supercells can be predicted by Eq. (17). Although the obtained hardness results have significant difference compared with those obtained by the bond order model, it does not affect the analysis of hardness variation in Mo_2CoB_2 crystals after doping with transition metal elements. The hardness prediction results are shown in Table 4, and Fig. 5 shows the hardness of doped transition metal element *X* at different sites in the Mo_2CoB_2 supercell.

The hardness values obtained from Eq. (17) only consider the intrinsic hardness of the doped models and do not consider the effects of lattice distortion caused by doping on defects, such as dislocations in the material. As shown in Fig. 5, without considering the influence of dislocations in the material, the intrinsic hardness of all doped models is lower than that of the undoped model. Moreover, the hardness variation in doped models is basically consistent with the variation of Debye temperature. With increasing the atomic number, the hardness of doped elements occupying Mo sites is firstly increased and then decreased. The highest hardness value is obtained when the doped element is V element. Similarly, when the transition metal element occupies the Co site, the maximum hardness is achieved for the Fe element.

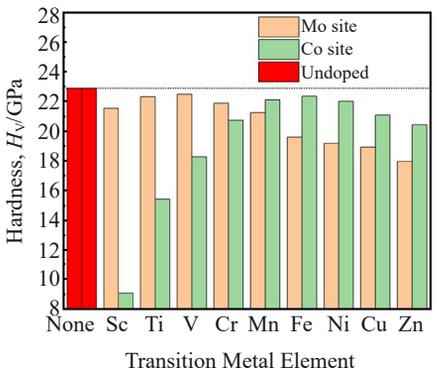

Fig.5 Hardness of doped transition metal element *X* at different sites in Mo_2CoB_2 supercell (dashed line represents the hardness value of undoped model)

All transition metal elements tend to have higher hardness when they occupy their preferred atomic sites. For example, the hardness of Sc (strong), Ti (strong), and V (weak) elements occupying Mo sites is much higher than that occupying the Co sites. In contrast, the hardness of Mn (weak), Fe (weak), Ni (strong), Cu (weak), and Zn (weak) elements occupying the Co sites is much higher than that occupying the Mo sites. This may be related to the stability of the crystal structure and the strength of chemical bonds. When the transition metal elements occupy their preferred sites, the stability is better, resulting in stronger chemical bonds.

However, it should be noticed that when Cr occupies its preferential Co site, the hardness is lower than that occupying the Mo site. There are two reasons for this phenomenon. Firstly, the $\tilde{E}_X^{\mathrm{Mo}\rightarrow\mathrm{Co}}$ value of Cr calculated by Eq.(7) is 0.481, which is close to 0.5. $E_{\mathrm{Cr}}^{\mathrm{Mo}\rightarrow\mathrm{Co}}$ and $E_{\mathrm{Cr}}^{\mathrm{Co}\rightarrow\mathrm{Mo}}$ values are basically the same, suggesting that the energy for Cr movement from Mo sites to Co sites is extremely close to that from Co sites to Mo sites. In this case, Cr element can occupy both sites. Hu et al[46] studied the effects of Cr element doping into Mo_2FeB_2-Fe ternary borides, and the results showed that Cr element can appear at both binder phase Fe and hard phase Mo_2FeB_2. Moreover, Yang et al[8] found that Cr can also appear at binder phase Co and hard phase MoCoB in the MoCoB-Co ternary borides. In this case, it can be deduced that Cr tends to occupy both sites. Additionally, when Cr element is doped into the MoCoB-Co ternary borides, the volume fraction of binder phase is decreased with increasing the Cr addition, and there is no big difference for the hard phase. It can be noticed that Cr element tends to form a third phase with Co element, which presents low hardness and low fracture toughness. Hence, it can be inferred that Mo_2CoB_2 shows low hardness when Cr occupies the Co site.

3 Conclusions

1) Through the cohesive energy and formation enthalpy, all doped MoCoB*X* compounds are thermodynamically stable. Moreover, all doped models are mechanically stable with the consideration of Born-Huang's criterion.

2) The point defect theory is the optimal criterion to determine the occupation of dopant elements in the Mo_2CoB_2 crystal cell. Sc and Ti elements have strong Mo site preference, and V element has a weak Mo site preference. Cr, Mn, Fe, Cu, and Zn elements have a weak Co site preference, and Ni element has a strong Co site preference.

3) The Debye temperature of $Mo_7TiCo_4B_8$, $Mo_7VCo_4B_8$, and $Mo_7CrCo_4B_8$ models is higher than that of the undoped model, whereas that of other doped models are lower than that of the undoped model. Therefore, in the preparation of Mo_2CoB_2-based cermet, except Ti, V, and Cr elements, the addition of transition metal elements of large quantity into the Mo_2CoB_2 hard phase should be avoided.

4) With the consideration of crystal structure, when the transition metal elements occupy their preferential sites, they exhibit higher hardness, except for the Cr element. Moreover, the hardness of all doped models is lower than that of the undoped model.

References

1 Tinklepaugh J R, Crandall W B. *Cermet*[M]. Shanghai: Shanghai Scientific & Technical Publisher, 1964: 8

2 Liu Futian, Huang Weiling, Li Wenhu *et al*. *Materials Science and Technology*[J], 2005, 13(5): 355 (in Chinese)

3 Shepeleva L, Medres B, Kaplan W D *et al*. *Surface and Coatings Technology*[J]. 2000, 125(1–3): 45

4 Sailer B, Pjetursson E, Zwahlen M *et al*. *Clinical Oral Implants Research*[J], 2007, 18(3): 86

5 Zhang Liehua, Fang Zhigang Zak, Xu Lin *et al*. *Heat Treatment of Metals*[J], 2016, 41(2): 84 (in Chinese)

6 Cao Fei, Yang Huipeng, Wang Wei *et al*. *Conservation and Utilization of Mineral Resources*[J], 2018, 38(2): 145 (in Chinese)

7 Tong Chuangchuang. *Effects of Cr, Ni, and Mn on Mechanical Properties of Mo2FeB2 Based on First Principles*[D]. Chengdu: Southwest Petroleum University, 2017 (in Chinese)

8 Yang Guoqiang. *Design and Preparation of High Hardness Ternary Boride Basic Ceramics*[D]. Beijing: University of Science and Technology Beijing, 2020

9 Takagi K I. *Journal of Solid State Chemistry*[J], 2006, 179(9): 2809

10 Sáez A, Arenas F, Vidal E. *International Journal of Refractory Metals and Hard Materials*[J], 2003, 21(1–2): 13

11 Andreas L J, Helmuth K, Peter R *et al*. *Journal of the Japan Institute of Metals*[J], 2000, 64(2): 154

12 Hirata H, Iwanaga K, Yamazaki Y *et al*. *Journal of the Japan Society of Powder and Powder Metallurgy*[J], 2006, 53(5): 447

13 Pan Yingjun, Xu Ming, Hu Bing *et al*. *Journal of Wuhan University of Science and Technology*[J], 2011, 34(2): 96 (in Chinese)

14 Jian Y X, Huang Z F, Liu X T *et al*. *Results in Physics*[J], 2019, 15: 102 698

15 Zhang Shunmeng, Xiong Kai, Jin Chengchen *et al*. *Rare Metal Materials and Engineering*[J], 2022, 51(12): 4533 (in Chinese)
16 Lin Y H, Tong C C, Pan Y *et al*. *Modern Physics Letters B*[J], 2017, 31(12): 1 750 138
17 Wang S L, Pan Y, Lin Y H *et al*. *Computational Materials Science*[J], 2018, 146: 18
18 Zhang T, Yin H Q, Zhang C *et al*. *Modern Physics Letters B*[J], 2018, 32(21): 1 850 240
19 Zhang T, Yin H Q, Zhang C *et al*. *Materials*[J], 2019, 12(6): 967
20 Zhang T, Yin H Q, Zhang C *et al*. *Chinese Physics B*[J], 2018, 27(10): 107 101
21 Hohenberg P, Kohn W. *Physics Review*[J], 1964, 136(3B): B864
22 Kohn W, Sham L J. *Physics Review*[J], 1965, 140(4A): A1133
23 Kresse G, Furthmüller J. *Physical Review B*[J], 1996, 54(16): 11 169
24 Kresse G, Furthmüller J. *Computational Materials Science*[J], 1996, 6(1): 15
25 BlÖchl P E. *Physical Review B*[J], 1994, 50(24): 17 953
26 Kresse G, Joubert D. *Physical Review B*[J], 1999, 59(3): 1758
27 Perdew J P, Burke K, Ernzerhof M. *Physical Review Letters*[J], 1996, 77(18–28): 3865
28 Chen M, Wang C Y. *Scripta Materialia*[J], 2009, 60(8): 659
29 Keränen J, Stenberg T, Mantyla T *et al*. *Surface and Coatings Technology*[J], 1996, 82(1–2): 29
30 Li Jian, Zhang Ming. *Journal of Alloys and Compounds*[J], 2013, 556: 214
31 Ruban A V, Skriver H L. *Solid State Communications*[J], 1996, 99(11): 813
32 Ruban A V, Skriver H L. *Physical Review B*[J], 1997, 55(2): 856
33 Jiang C, Gleeson B. *Scripta Materialia*[J], 2006, 55(5): 433
34 Kim D E, Shang S L, Liu Z K. *Intermetallics*[J], 2010, 18(6): 1163
35 Xu W W, Wang Y, Wang C P *et al*. *Scripta Materialia*[J], 2015, 100: 5
36 Mouhat F, Coudert F X. *Physical Review B*[J], 2014, 90(22): 224 104
37 Jian Y X, Huang Z F, Xing J D *et al*. *Materials Chemistry and Physics*[J], 2019, 221: 311
38 Ravindran P, Fast L, Korzhavyi P A *et al*. *Journal of Applied Physics*[J], 1998, 84(9): 4891
39 Liang Y F, Shangetal S L. *Intermetallics*[J], 2011, 19(10): 1374
40 Hill R. *Proceedings of the Physical Society, Section A*[J], 1952, 65(5): 349
41 Pan Y. *Journal of Alloys and Compounds*[J], 2019, 779: 813
42 Chen X Q, Niu H Y, Li D Z *et al*. *Intermetallics*[J], 2011, 19(9): 1275
43 Pugh S F. *The London, Edinburgh, and Dublin Philosophical Magazine and Journal of Science*[J], 1954, 45(367): 823
44 Haque E, Hossain M A. *Journal of Alloys and Compounds*[J], 2018, 730: 279
45 Lv Z L, Cui H L, Huang H M *et al*. *Journal of Alloys and Compounds*[J], 2017, 692: 440
46 Hu Bing, Pan Yingjun, Wang Qingfang *et al*. *Heat Treatment of Metals*[J], 2011, 36(6): 29 (in Chinese)

基于第一性原理的Mo_2CoB_2三元过渡金属硼化物掺杂效应研究

张宇瀚，金　娜，刘　颖
(四川大学 材料科学与工程学院 稀土钒钛材料中心，四川 成都 610065)

摘　要：利用第一性原理计算研究了掺杂第四周期过渡金属元素对Mo_2CoB_2的结构、力学和热力学性质的影响。通过计算结合能和形成焓以及与Born-Huang标准比较，发现所有模型都满足力学与热力学稳定条件。采用点缺陷理论确定了掺杂元素在Mo_2CoB_2晶体中的占位以及占位偏好。结果表明，Sc和Ti对Mo点位表现出强烈的占位偏好，V对Mo点位仅有较弱的占位偏好。同时，Cr、Mn、Fe、Cu和Zn对Co点位具有较弱的占位偏好，而Ni对Co点位有较强的占位偏好。通过对比计算得到德拜温度，发现除$Mo_7TiCo_4B_8$、$Mo_7VCo_4B_8$和$Mo_7CrCo_4B_8$外，其他掺杂模型的德拜温度都低于未掺杂模型，这说明实验中应尽量避免在Mo_2CoB_2硬质相中大量添加除Ti、V和Cr以外的过渡金属元素。最后，除Cr掺杂模型外，其他掺杂模型的硬度计算结果都低于未掺杂的模型。同时，占据偏好点位的掺杂元素模型的硬度通常比占据非偏好点位的更高。本研究为开发性能更好的Mo_2CoB_2金属陶瓷提供了理论支持。

关键词：金属陶瓷；第一性原理；力学性能；M_2CoB_2-Co

作者简介：张宇瀚，男，1998年生，硕士，四川大学材料科学与工程学院稀土钒钛材料中心，四川 成都 610065，E-mail：zhangyuhans@stu.scu.edu.cn